Incorporation of Electrochemically Exfoliated Graphene Oxide and TiO$_2$ into Polyvinylidene Fluoride-Based Nanofiltration Membrane for Dye Rejection

A. B. Suriani · Muqoyyanah · A. Mohamed · M. H. D. Othman · R. Rohani · I. I. Yusoff ·
M. H. Mamat · N. Hashim · M. N. Azlan · M. K. Ahmad · P. Marwoto · Sulhadi ·
H. H. Kusuma · M. D. Birowosuto · H. P. S. Abdul Khalil

Abstract In this work, the novel direct synthesis method of dimethylacetamide-based graphene oxide (GO) was performed through electrochemical exfoliation assisted by commercially available single-tail sodium dodecyl sulphate (SDS) surfactant. Then, the synthesised GO (SDS–GO) was incorporated into polyvinylidene fluoride (PVDF) solution to produce a nanofiltration (NF) membrane through the phase immersion method. The addition of GO into the preparation of membrane solution alters the membrane morphology and improves the hydrophilicity. TiO$_2$ was also used as an additive for the NF membrane fabrication to further increase the membrane hydrophilicity. The fabricated PVDF/SDS–GO/TiO$_2$ and PVDF/SDS–GO NF membranes were compared with pure PVDF membrane. Then, the fabricated NF membranes were tested for methylene blue (MB) rejection with 10 ppm MB concentration. On the basis of the dead-

A. B. Suriani · Muqoyyanah · A. Mohamed · N. Hashim
Nanotechnology Research Centre, Universiti Pendidikan Sultan Idris, 35900 Tanjung Malim, Perak, Malaysia

A. B. Suriani (✉) · Muqoyyanah · M. N. Azlan
Department of Physics, Universiti Pendidikan Sultan Idris, 35900 Tanjung Malim, Perak, Malaysia
e-mail: absuriani@yahoo.com

A. Mohamed · N. Hashim
Department of Chemistry, Faculty of Science and Mathematics, Universiti Pendidikan Sultan Idris, 35900 Tanjung Malim, Perak, Malaysia

M. H. D. Othman
Advanced Membrane Technology Research Centre (AMTEC), Universiti Teknologi Malaysia, 81310 Skudai, Johor, Malaysia

R. Rohani · I. I. Yusoff
Department of Chemical and Process Engineering, Faculty of Engineering and Built Environment, Universiti Kebangsaan Malaysia (UKM), 43600 Bangi, Selangor, Malaysia

M. H. Mamat
NANO-ElecTronic Centre (NET), Faculty of Electrical Engineering, Universiti Teknologi MARA (UiTM), 40450 Shah Alam, Selangor, Malaysia

M. K. Ahmad
Microelectronic and Nanotechnology-Shamsuddin Research Centre (MiNT-SRC), Faculty of Electrical and Electronic Engineering, Universiti Tun Hussein Onn Malaysia, Parit Raja, 86400 Batu Pahat, Johor, Malaysia

P. Marwoto · Sulhadi
Materials Research Group, Thin Film Laboratory, Faculty of Mathematics and Natural Science, Universitas Negeri Semarang (UNNES), Sekaran, Gunungpati, Semarang 50229, Indonesia

H. H. Kusuma
Physics Department, Faculty of Sciences and Technology, Universitas Islam Negeri, Walisongo Semarang, Central Java, Indonesia

M. D. Birowosuto
CNRS International NTU Thales Research Alliance (CINTRA), Research Techno Plaza, 50 Nanyang Drive, Border X Block, Singapore 637553, Singapore

H. P. S. A. Khalil
Wood, Paper and Coating Division, School of Industrial Technology, Universiti Sains Malaysia, 11800 Pulau, Pinang, Malaysia

🌲 Springer

end cell measurement operated at the pressure of 2 bar, the PVDF/SDS–GO/TiO$_2$ presents high MB rejection (92.76%) and the highest dye flux (7.770 L/m^2 h). This dye flux value was sevenfold higher than that of pure PVDF membrane (1.146 L/m^2 h) which was due to the utilisation of both GO and TiO$_2$ that improved the membrane hydrophilicity as indicated by the lowest contact angle (64.0 ± 0.11°). High porosity (57.46%) also resulted in the highest water permeability (4.187 L/m^2 h bar) of the PVDF/SDS–GO/TiO$_2$ NF membrane.

1 Introduction

The rapid industrial factory growth caused huge problems, such as polluted air and water, from its waste products which are mainly caused by the high amount of dangerous heavy metal and dye waste that are dissolved in air and water, respectively. This contamination results from the textile, pharmaceutical, metal-plating and printing industries which causes the lack of clean water. The difficulty in treating dye wastewater, which contains toxic substances and are non-degradable substances, becomes an important issue that needs to be solved (Zhu et al. 2017). Several methods that are generally used to remove dye from contaminated water are chemical and physical sorption (Darwish et al. 2019), evaporation, biological degradation, chemical oxidation, flocculation–coagulation, photocatalytic system (Rashad et al. 2016), electrodeposition and membrane separation/filtration (Makertihartha et al. 2017; Zhu et al. 2017). Among these methods, membrane filtration gains considerable interest due to its several advantages, such as simple operation, minimal chemical used, low energy, good separation, easy automation, low pollution and high recovery rate (Méricq et al. 2015; Zhu et al. 2017).

The pollutant filtration efficiency is strongly affected by the membrane type. The membrane can be divided into microfiltration, ultrafiltration, nanofiltration (NF) and reverse osmosis (RO) on the basis of its pore size (Shon et al. 2013). NF membrane offers some advantages for textile wastewater, such as relatively high water flux and permeability compared with RO, low

operating pressure, low energy consumption, small pore size (1–5 nm) and high efficiency to remove the dye (Safarpour et al. 2015; Shon et al. 2013; Zhu et al. 2017). Several methods that are generally used to prepare the membrane include interfacial polymerisation, stretching, sintering, track-etching, electrospinning and phase inversion methods (Mokhtar et al. 2015). Phase inversion method is commonly used due to its simple and easy preparation. Then, the morphology of the fabricated membrane is strongly affected by several factors, including polymer concentration, solvent (Madaeni and Taheri 2011; Nasib et al. 2017), non-solvent (Thürmer et al. 2012), composition, coagulant temperature (X. Wang et al. 2008), precipitation time, temperature and evaporation time before immersion, additive (Mokhtar et al. 2015; Ngang et al. 2012) and casting thickness (Madaeni and Taheri 2011).

Various polymer materials that are generally used for membrane fabrication include polysulfone, polyacrylonitrile, polyaniline (Yusoff et al. 2018), polystyrenesulfonate, polyethersulfone (Zinadini et al. 2014), polymethylmethacrylate, polyethyleneimine, polyvinylpyrrolidone and polyvinylidene fluoride (PVDF) (Cao et al. 2006; Kumaran et al. 2015; Ngang et al. 2012; Zhu et al. 2017). The formation of membrane pores with either finger- or sponge-like structure is also affected by the membrane solution viscosity (Nasib et al. 2017). These properties are strongly affected by the polymer material and solvent types. An extremely low polymer molecular weight results in exceedingly weak membrane, whereas an excessively high value makes the membrane difficult to process due to the highly viscous solution (Kim et al. 2017). PVDF presents excellent properties, including chemical, alkali and corrosion resistance; thermal, chemical and UV stability; good membrane-forming properties; high mechanical strength and good solubility in many organic solvent, thereby making it applicable for water treatment (Ngang et al. 2012; Nikooe and Saljoughi 2017; Wang et al. 2012; Zhu et al. 2017). Meanwhile, several generally used organic solvents include N-methyl-2-pyrrolidone (NMP) (Nasib et al. 2017; Thuyavan et al. 2016), DMF (Thürmer et al. 2012), dimethylsulfoxide (Thuyavan et al. 2016) and dimethylacetamide (DMAc) (Madaeni and Taheri 2011; Nasib et al. 2017; Thuyavan et al. 2016).

Madaeni et al. investigated the effect of polymer concentration, casting thickness and solvent type on the morphology of the fabricated membrane. The result

showed that 20 wt% of PVDF presents wider and longer finger-like pore morphology than those with lower PVDF content. These researchers also found that 200-μm casting thickness results in the highest flux and permeability (Madaeni and Taheri 2011). DMAc utilisation in the membrane solution preparation results in high porosity and flux compared with NMP and DMF (Nasib et al. 2017; Thuyavan et al. 2016; Wang et al. 2008). Meanwhile, Buonomenna et al. showed that the direct immersion in the coagulant after casting process results in higher porosity than that of delayed immersion. Membrane solution heating during stirring process also resulted in higher porosity membrane than the room temperature stirring process (Buonomenna et al. 2007). Thürmer et al. also found that the use of pure water as coagulant results in an asymmetric pore membrane with higher hydrophilicity than ethanol, followed by a water coagulant (Thürmer et al. 2012).

However, PVDF is a well-known high hydrophobic material which reduces the flux and permeability, thereby requiring modification either through physical or chemical means (Cao et al. 2006). In improving PVDF hydrophilicity, hydrophilic inorganic nanoparticle additives, such as Al_2O_3, black Fe_3O_4, CdS, silica and C-based and semiconductor materials, are clearly needed. Carbon nanotubes, graphene, graphene oxide (GO) and reduced GO which are C-based materials are widely investigated for PVDF modification. Among these materials, GO gained considerable interest due to its large surface area and high amount of O functional groups. Zhu et al. obtained higher hydrophilicity and water flux than pure PVDF membrane by adding GO. GO addition also alters the membrane morphology of the finger-like structure (Zhu et al. 2017). Zhao et al. showed that PVDF/GO blend membrane presents higher rejection than that of pure PVDF membrane (Zhao et al. 2013). This result also agreed with the findings of other studies (Hu and Mi 2013; Xu et al. 2014; Zhang et al. 2017).

Most studies reported the use of the powder form of GO that resulted from the Hummers' method as additives in membrane solution preparation (Hu and Mi 2013; Wang et al. 2012; Zhao et al. 2013). The synthesised GO by Hummers' or modified Hummers' method produced good-quality GO. However, it presents unsafe and inefficient synthesis method due to the usage of strong acid and highly toxic material and its complex synthesis steps (Kang et al. 2016). In limiting these drawbacks, a simple and safe GO synthesis method needs to be developed. Electrochemical exfoliation

method is a promising solution due to its simple, low cost and low chemical consumption (Yu et al. 2015). Chemicals, such as acids and sulfurics, and even water can be used as electrolyte for the synthesis process (Liu et al. 2015; Parvez et al. 2013; Yu et al. 2015). Suriani et al. used this method by using water as electrolyte and assisted by a surfactant for GO layer intercalation and dispersion (Suriani et al. 2015, 2018b, c). These researchers used the produced GO-based solution to fabricate thin film and yield a relatively high conductivity (Suriani et al. 2016). The results showed that low synthesis and thin film fabrication steps were achieved compared with the Hummers' method. These researchers also reported the successful in situ method of producing natural rubber latex (NRL)–GO nanocomposite by intermixing NRL and water-based electrolyte through electrochemical exfoliation (Suriani et al. 2015). High conductivity and capacitance value were achieved when the fabricated NRL–GO nanocomposite electrode was used for supercapacitor application (Suriani et al. 2016).

Meanwhile, several metal oxides, such as ZnO, ZrO_2 and TiO_2, were widely developed as an additive due to their good properties, such as stability, availability, antibacterial activity and the presence of abundant hydroxyl groups. The abundance of hydroxyl groups improves the hydrophilicity of the material, thereby increasing the flux and permeability (Cao et al. 2006). Ngang et al. showed that PVDF–TiO_2-mixed matrix membrane enhances the water permeability and increases the methylene blue (MB) rejection (Ngang et al. 2012). Hence, in this work, the directly synthesised DMAc-based GO assisted by commercially available single-tail sodium dodecyl sulphate (SDS) surfactant was used as a solvent before mixing it with TiO_2 nanoparticles (NPs) as an additive to fabricate the PVDF/SDS–GO/TiO_2 membrane. TiO_2 was utilised to improve the hydrophilicity of the membrane further. Then, pristine PVDF membrane that was fabricated by DMAc and PVDF/SDS–GO that was fabricated using the directly synthesised DMAc-based GO were used for comparison. Afterward, the three fabricated membranes were used to investigate their effectiveness for MB rejection application. To the best of our knowledge, this work presents a novel and simple GO synthesis through electrochemical exfoliation assisted by SDS surfactant by utilising DMAc as the solvent for PVDF-based membrane fabrication.

2 Materials and Methods

2.1 Materials

Commercially available SDS (Sigma-Aldrich) surfactant, DMAc and graphite rods (99.99%, 150 mm in length and 10 mm in diameter, GoodFellow GmbH, Germany) were used in GO synthesis. PVDF (Kynar 760, grade in palette form) and titanium (IV) oxide ($\geq$ 99.5%, Sigma-Aldrich) were used as the main polymer material and an additive in the NF membrane fabrication, respectively. MB (Sigma-Aldrich) was used for the dye rejection test.

2.2 DMAc-Based GO Synthesis

GO was synthesised through electrochemical exfoliation as mentioned in previous works (Suriani et al. 2018a, b, c). However, this work utilised DMAc to replace water as the electrolyte. In brief, SDS was dissolved in DMAc to form 0.1 M of the electrolyte. Then, two graphite rods were used as working and counter electrodes which are partially immersed and connected to the DC power supply (7 V) for 24 h of synthesis.

2.3 PVDF-Based NF Membrane Fabrication

The synthesised SDS–GO was further used to prepare the casting solution. The TiO$_2$ and PVDF were dissolved to the DMAc_SDS–GO solution and stirred at 70 °C for 24 h. Meanwhile, pure PVDF membrane was only dissolved to DMAc for comparison. The weight percentage data of the fabricated membrane are presented in Table 1. Then, well-mixed membrane was kept at room temperature overnight to remove the air bubbles. Then, fully degassing membrane solution was casted using casting knife on a glass plate with 200-μm casting gap. Afterward, casted membrane was directly immersed in the coagulation bath of DI water overnight, and the membrane was kept by soaking it in DI water until further characterisation.

2.4 Membrane Characterisation

The morphology of the fabricated membranes (top and cross-section) was examined through field emission scanning electron microscopy (Hitachi SU8020). Liquid nitrogen immersion was performed prior to FESEM observation to obtain a good membrane fracture for cross-sectional observation. Prior to the test, the membrane surface was coated by thin gold. The elemental composition of the samples was directly confirmed by an EDX instrument (Horiba EMAX). The structural properties of the fabricated NF membranes were studied through micro-Raman spectroscopy (Renishaw InVia microRaman System). The hydrophilicity of the fabricated membrane was investigated by placing the dry membrane on a glass slide and conducting drop shape analysis (DSA100, KrussGmbH, Germany). The membrane porosity was determined through gravimetric method by using the following equation:

$$\varepsilon = \frac{(w_1 - w_2)/\rho_w}{[(w_1 - w_2)/\rho_w] + (w_2/\rho_p)} \times 100\% \qquad (1)$$

where ε is membrane porosity (%), w_1 and w_2 are the wet and dry membrane weights (g), respectively, ρ_w is the water density (0.998 g/cm^3), and ρ_p is the PVDF density (1.78 g/cm^3).

Water flux and dye rejection were measured in a dead-end stirred cell (Sterlitech HP4750) with a capacity of 300 mL, as illustrated in Fig. 1. The disc membrane had diameter of 49 mm with an active area of the measured membrane of 14.6 cm^2. Water flux was measured under 5 different pressure levels (1–5 bar) with 10-min measurement for each pressure. Then, flux was measured using the following equation:

$$J = \frac{V}{A\Delta t} \qquad (2)$$

where J is the permeated flux (L/m^2 h), V is the permeated water volume (m^3), A is the membrane area (m^2) and Δt is the operating time (h). Next, dye rejection test was performed at the pressure of 2 bar at the pressure of 10 ppm in MB solution. UV–vis was also used to measure the adsorption of the treated dye solution. Then, the dye rejection efficiency (R) was calculated using the following equation (Ngang et al. 2012):

$$R\,(\%) = \left[1 - \frac{C_p}{C_o}\right] \times 100\% \qquad (3)$$

where R is the dye rejection efficiency (%), C_p is the permeate dye concentration (ppm) and C_o is the initial dye concentration (ppm).

Table 1 Material weight percentage for the PVDF-based NF membrane fabrication

| Membrane	Material (wt%)			
	PVDF	DMAc_SDS-GO	DMAc	TiO$_2$
PVDF/SDS-GO/TiO$_2$	20	79	–	1
PVDF/SDS-GO	20	80	–	–
PVDF	20	–	80	–

3 Results and Discussion

3.1 FESEM and EDX Analysis

The difference in the morphology of the fabricated NF membranes (PVDF, PVDF/SDS–GO and PVDF/SDS–GO/TiO$_2$) was significant, as shown in Fig. 2. Overall, all fabricated membranes presented an asymmetric structure consisting of porous finger-like and dense sponge-like pores in the top- and sublayers, respectively. These structures were formed due to the high miscibility of DMAc and DI water as the solvent and non-solvent pair which generates the pores, respectively (Buonomenna et al. 2011). The dark and smooth skin layer of the PVDF membrane was clearly seen from its top surface (Fig. 2a). The membrane surface instantly solidifies during coagulation when the casting solution is immersed to DI water (Nawi et al. 2018; Zhu et al.

2017). The cross-section of the membrane surface shown in Fig. 2b revealed that the top membrane sublayer consisted of extremely porous and wide finger-like pores structure with spherical shape in its bottom. The top membrane sublayer pore size was observed ranging from 661 nm to 9.59 μm. The PVDF membrane also showed thin and coarse pore walls. Meanwhile, the bottom sublayer pores presented large sponge-like structure with pore size varying from 772 nm to 1.87 μm. On the basis of high-magnification observation, the distance of the shortest membrane pores from its surface was 694 nm (Fig. 2c). Further EDX analysis showed high atomic percentages of F (55.15%) and C (44.79%) as the components of PVDF (Fig. 2d).

A slightly rough membrane surface was observed for the PVDF/SDS–GO sample. The SDS–GO sheets were homogeneously spread all over the sample, as pointed

Fig. 1 Dead-end stirred cell used to measure the water flux and dye rejection
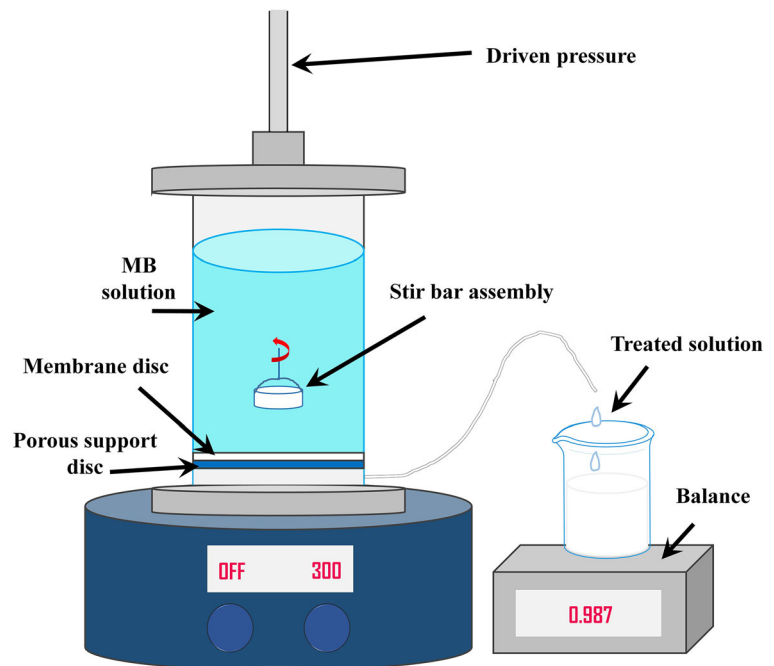
Fig. 2 FESEM images and EDX analysis of the fabricated NF membrane; PVDF (**a**–**d**), PVDF/SDS-GO (**e**–**h**) and PVDF/SDS-GO/TiO$_2$ (**i**–**l**)
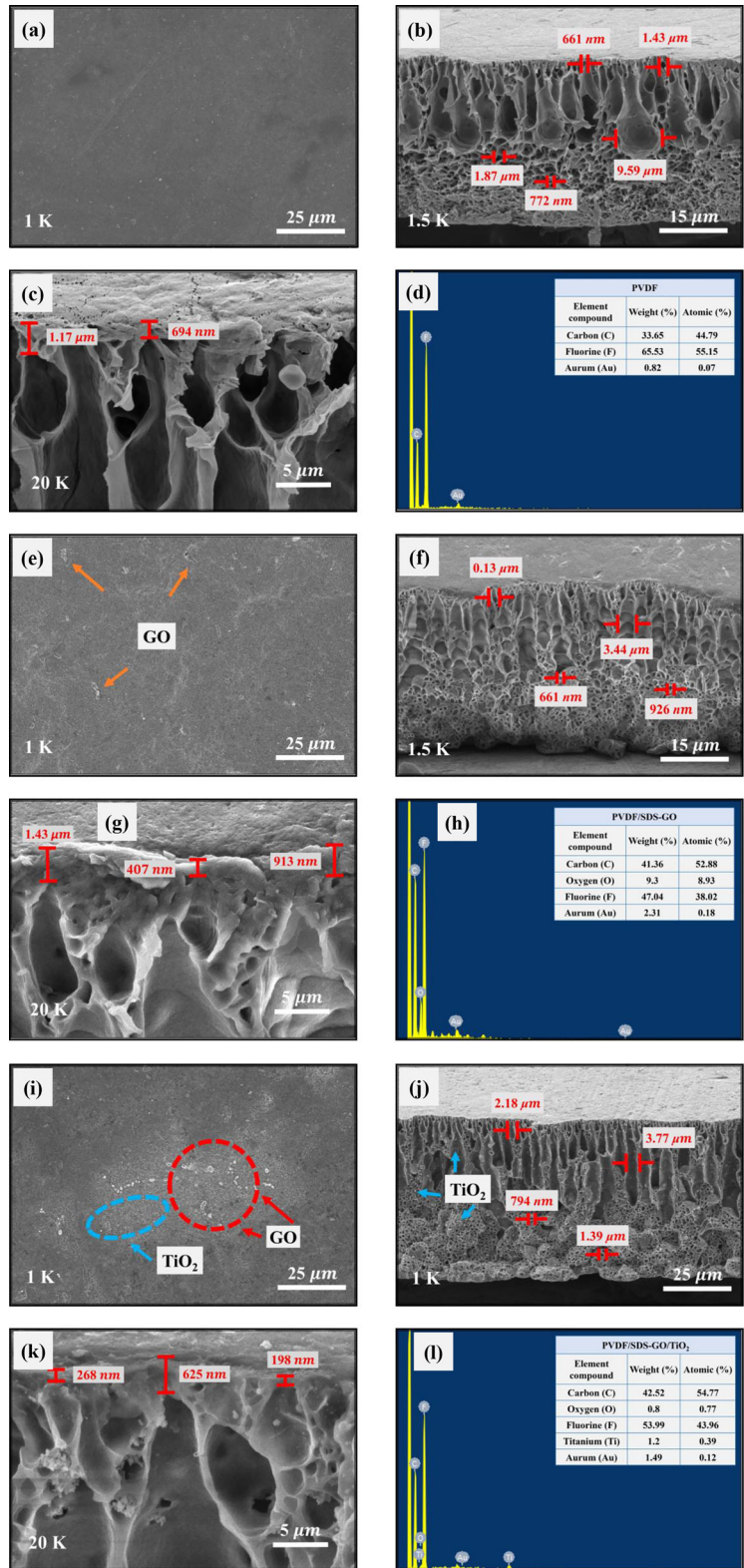
by the orange arrows in Fig. 2e. However, the membrane surface was smooth without any crack, thereby confirming the good stability of the fabricated GO-based membranes (Zinadini et al. 2014). The addition of SDS–GO strongly altered the membrane morphology, as shown by its cross-section which presented more homogeneous porous size than the PVDF sample. Highly porous structure density with a typical asymmetric finger-like structure was clearly observed, whilst its bottom sublayer showed small sponge-like structure with spherical shape (Fig. 2f). This finding was due to the hydrophilic groups contained in the SDS–GO which accelerated the solidification rate during the phase inversion method (Zhu et al. 2017). The top membrane sublayer pores ranged from ~ 0.13 to 3.44 μm, whilst the bottom membrane sublayer showed small membrane pores (~ 661–926 nm). The top PVDF/SDS–GO wall was clearly thicker than that of PVDF. The shortest pore distance from the membrane surface was 407 nm which was thinner than that of the PVDF sample (Fig. 2g). The higher C atomic percentage of PVDF/SDS–GO (52.88%) than that of the PVDF sample (44.79%) and O (8.93%) confirmed the presence of SDS–GO in this sample (Fig. 2h).

When TiO_2 was added, the colour of the membrane surface became lighter, as shown by the blue circle. The SDS–GO sheet was also evident in this sample, as shown by red circle in Fig. 2i. Arranged column-shaped finger-like pores were clearly observed in the PVDF/SDS-GO/TiO_2 sample from its cross-section view with slightly larger membrane pores in both the top (~ 2.18–3.77 μm) and bottom (~ 794 nm to 1.39 μm) sublayers than the PVDF/SDS–GO membrane. TiO_2 NPs were uniformly distributed all over the sample, as pointed by the blue arrows in Fig. 2j. A shorter pore distance from the membrane surface layer of PVDF/SDS–GO/TiO_2 (198 nm) was observed than those of PVDF/SDS–GO (407 nm) and PVDF (694 nm, Fig. 2k). The addition of both hydrophilic GO and TiO_2 in the membrane solution preparation also affected the thickness of the fabricated membrane which was confirmed by the thicker PVDF/SDS-GO/TiO_2 sample (60.1 μm) than of the PVDF (41.5 μm) due to the instantaneous demixing process during coagulation (Nikooe and Saljoughi 2017). Further EDX analysis confirmed Ti, O, C and F as the components of the sample, where the C atomic percentage presented a similar value (54.77%) with the PVDF/SDS–GO sample (52.88%). The atomic percentage of Au for all

samples (~ 0.07–0.18%) was due to the thin coating for FESEM analysis.

3.2 Micro-Raman Spectroscopy

Micro-Raman spectroscopy can be used to study the crystalline and polymeric membrane structures, such as the functional groups, group structure and the changes in the structural parameter when the polymer was modified (Hilal et al. 2017). The Raman spectra of the fabricated membranes are presented in Fig. 3. Several peaks as the characteristics of the PVDF matrix were clearly observed in the range of 150–1650 cm^{-1} (bottom graph). Two peaks at around 610.12 and 794.76 cm^{-1} were due to the CF_2 vibrations and related to the α phase of PVDF (Al-gharabli et al. 2017; Elashmawi and Gaabour 2015; Ghaffar et al. 2018; Kumaran et al. 2015). Meanwhile, other two peaks located at 838.46 and 1426.66 cm^{-1} were related to β phase of PVDF caused by phase combination of CH_2 rocking and CF_2 stretching mode (Al-gharabli et al. 2017; Bohara et al. 2017; Elashmawi and Gaabour 2015; Ghaffar et al. 2018; Kumaran et al. 2015). When SDS–GO was used as the solvent, the D- and G-bands which are characteristic of GO were clearly observed at 1332.42 and 1577.95 cm^{-1}, respectively (middle graph). The intensity ratio of D- and G-bands which is known as the I_D/I_G ratio can be used to investigate the defect level of the sample (Zhou et al. 2013). On the basis of the middle graph, the I_D/I_G ratio of the PVDF/SDS–GO membrane was 1.13, thereby indicating a high defect level of the synthesised GO. This phenomenon was due to the existence of oxygen functional groups resulting from the oxidation process during electrochemical exfoliation (Yu et al. 2015). The existence of TiO_2 on the PVDF/SDS–GO/TiO_2 membrane was confirmed by the several peaks located at 148.11, 395.70, 514.45 and 637.21 cm^{-1} which corresponded to the E_g, B_{1g}, A_{1g} and E_g modes of the anatase phase of TiO_2, respectively (top graph) (Balachandran and Eror 1982). The existence of GO was also confirmed by the D- and G-bands located at 1331.97 and 1575.08 cm^{-1}, respectively which also presented the same I_D/I_G ratio (1.13) as that of the PVDF/SDS–GO membrane. The unobserved PVDF peaks in the PVDF/SDS–GO and PVDF/SDS–GO/TiO_2 membranes were caused by the low-intensity PVDF peak, as presented in bottom graph.
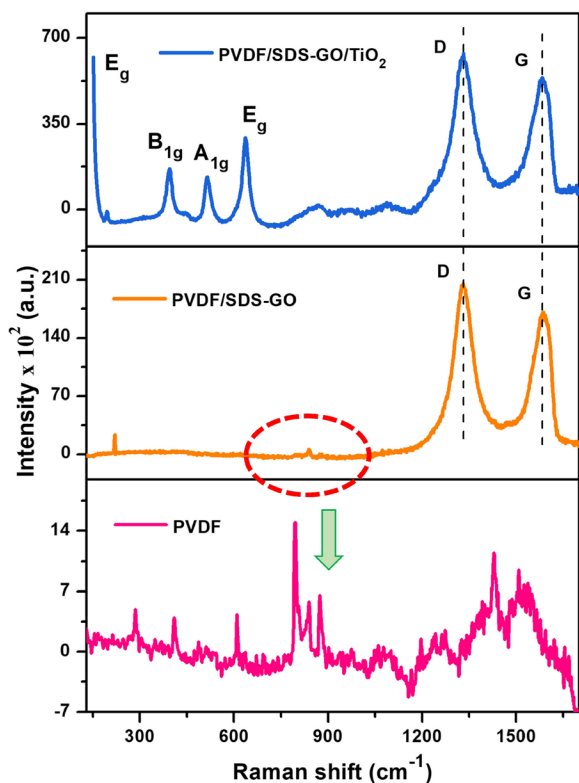
Fig. 3 Micro-Raman spectra of the fabricated PVDF-based NF membrane

3.3 Contact Angle Analysis and Porosity Measurement

To investigate the hydrophilicity which reflects the natural wettability of the fabricated membrane, contact angle analysis was performed, and the results are presented in Fig. 4. Clearly, the PVDF membrane presented the highest contact angle ($70.80 \pm 0.13°$), thereby indicating the hydrophobic nature of PVDF. The hydrophilicity improvement (low contact angle, $65.50 \pm 0.09°$) was obtained after SDS–GO utilisation (Fig. 4b). The GO migration to the membrane surface during membrane formation decorates the GO functional groups and improves membrane hydrophilicity (Zinadini et al. 2014). Low contact angle was further observed in the PVDF/SDS–GO/TiO$_2$ membrane ($64.0 \pm 0.11°$). The increased hydrophilicity was also contributed by the addition of TiO$_2$ which contains abundant hydroxyl groups and high affinity to water (Cao et al. 2006; Safarpour et al. 2015).

According to the calculation, the highest porosity was achieved by the PVDF membrane (61.52%) which due to the spherical membrane pore structure, as

presented in the FESEM images in Fig. 2b. Meanwhile, PVDF/SDS–GO presented lower porosity (50.96%) than the PVDF membrane due to the slimmer membrane top sublayer, as shown by the FESEM images in Fig. 2f. The fast inward diffusion of DI water during the coagulation process was caused by the hydrophilic groups of GO, thereby resulting in rapid membrane solidification (Zhu et al. 2017). High porosity (57.46%) was further achieved by adding TiO$_2$ (PVDF/SDS–GO/TiO$_2$). The presence of both hydrophilic GO and TiO$_2$ accelerated water penetration into the casted membrane due to the instantaneous demixing process, thereby increasing the precipitation rate of the casting solution and resulting in a porous membrane (Nikooe and Saljoughi 2017). The details of contact angle and porosity values are summarised in Table 2, as follows:

3.4 Water Flux on the Basis of Different Operating Pressure Levels

The water flux result of the fabricated NF membrane on the basis of different operating pressure is presented in Fig. 5. Clearly, the water flux increased linearly with the increase in pressure for all samples. High pressure resulted in increased driving force, thereby resulting in high permeate flux (Ngang et al. 2012). The lowest water permeability was exhibited by PVDF (1.099 L/m^2 h bar) due to its hydrophobic nature as confirmed by contact angle measurement. High water permeability (2.961 L/m^2 h bar) was further obtained by PVDF/SDS–GO due to its high hydrophilicity and short pore distance from the membrane surface. High hydrophilicity, which was also supported by the short pore distance, decreased the resistance, thereby increasing the water permeability by attracting water to and further through the membrane (Safarpour et al. 2015).

Then, the highest water permeability was achieved by PVDF/SDS–GO/TiO$_2$ (4.187 L/m^2 h bar) which can be attributed to the highest hydrophilicity that was calculated before. The abundant hydroxyl content of TiO$_2$ and the H-bond effect of F and O increased the water flux. The existence of GO also provided a channel for water flow, thereby increasing the flux. The defects on the GO edge plane act as the hydrophilic gate for the water to enter and then slip into the 2D nanometre channel due to C wall
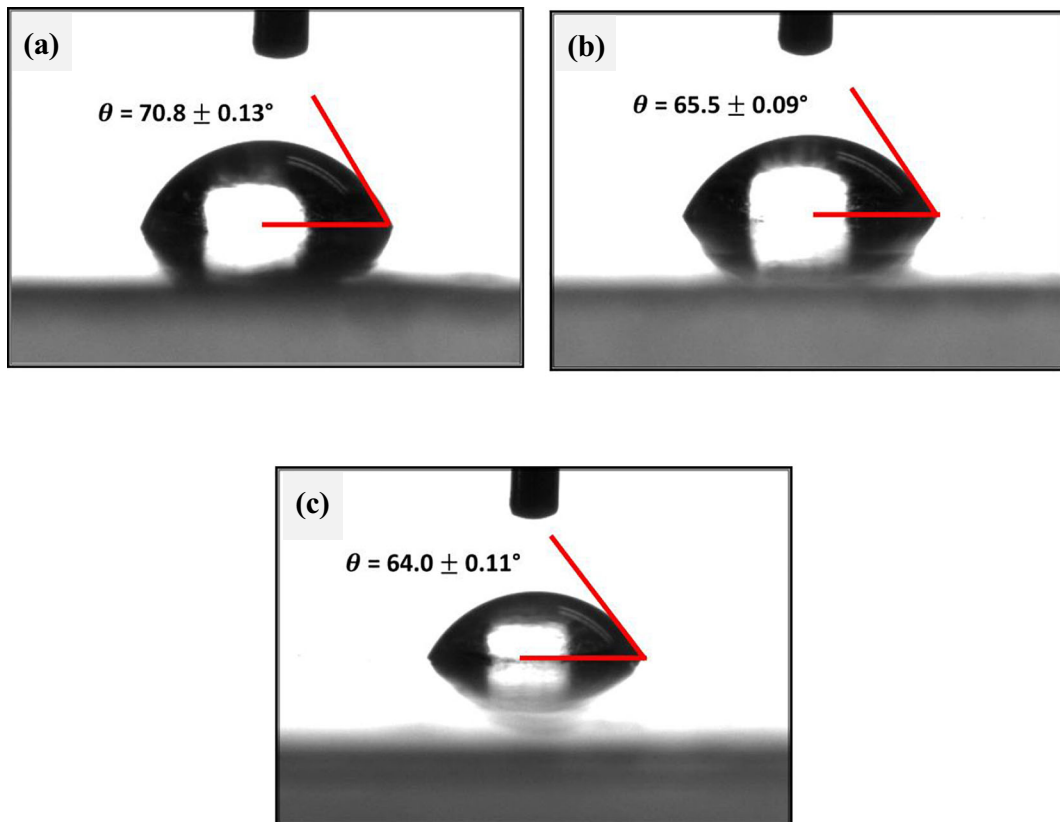
Fig. 4 Contact angle measurement of the fabricated NF membrane; PVDF (**a**), PVDF/SDS–GO (**b**) and PVDF/SDS–GO/TiO$_2$ (**c**)

hydrophobicity (Cao et al. 2006). The shortest pore distance from the membrane surface also supports this result. On the basis of the results, we can conclude that water flux and permeability were influenced by hydrophilicity and pore distance from the membrane surface. The water flux details of the fabricated NF membrane at different driving pressures are summarised in Table 3.

3.5 Dye Rejection Performance of the Fabricated NF Membrane

The filtration result of the 10 ppm MB dye at the pressure of 2 bar is presented in Fig. 6. Overall, all fabricated membranes showed the
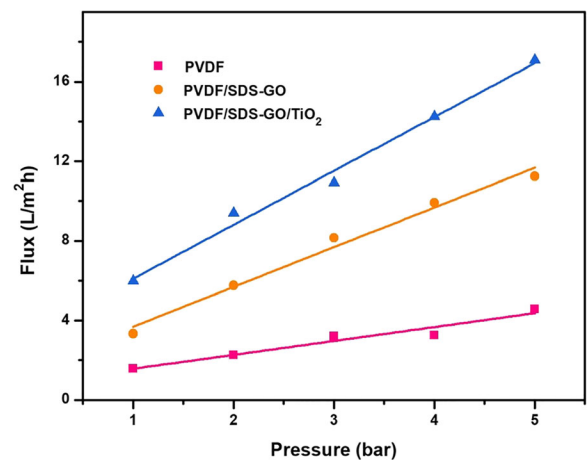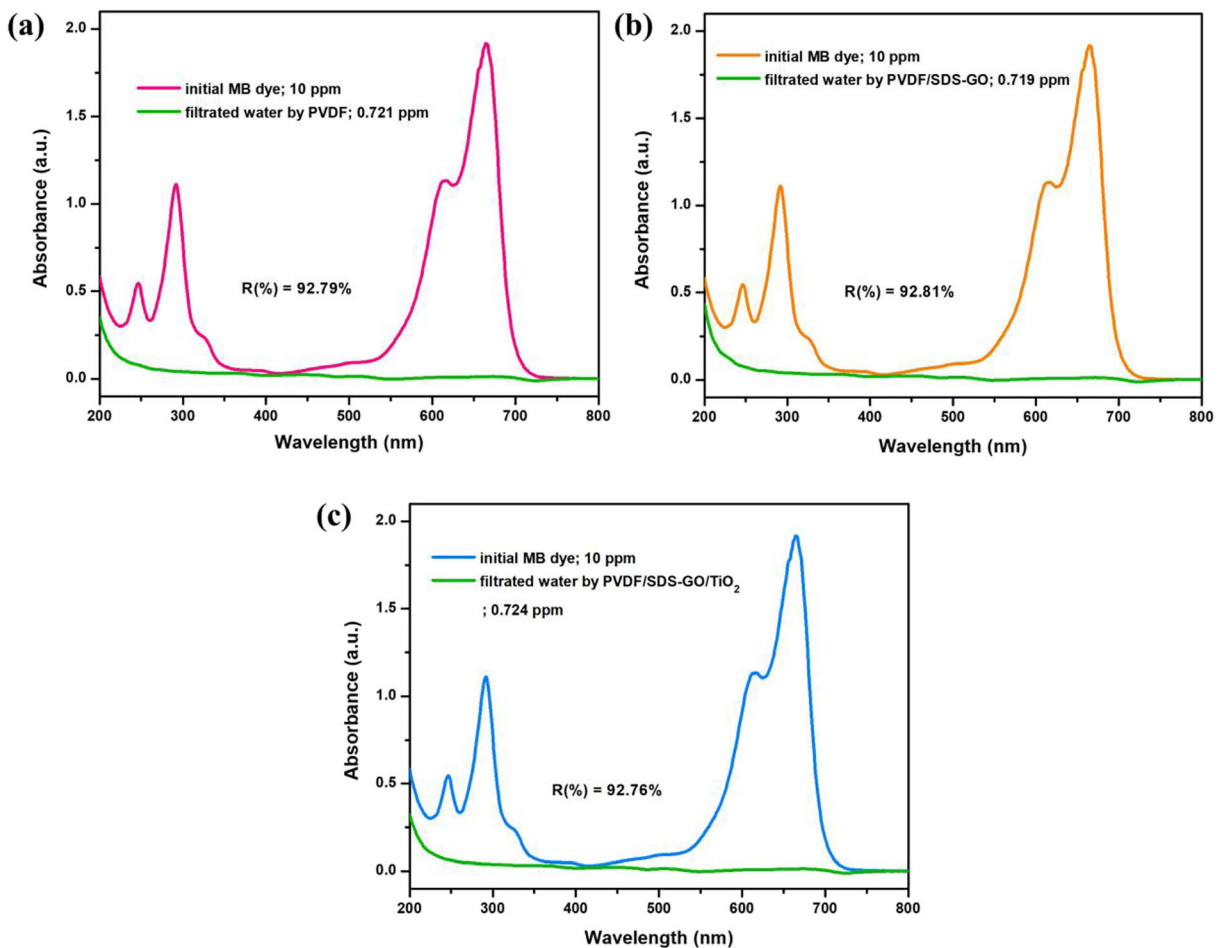

Fig. 5 Water flux measurement of the fabricated NF membrane on the basis of different driving pressure levels

Table 2 Contact angle and porosity values of the fabricated NF membranes

Membrane	Contact angle (°)	Porosity (%)
PVDF	70.8 ± 0.13	61.52
PVDF/SDS–GO	65.5 ± 0.09	50.96
PVDF/SDS–GO/TiO$_2$	64.0 ± 0.11	57.46

Table 3 Water flux details of the fabricated NF membrane on the basis on different pressure levels

Pressure (bar)	Water flux (L/m^2 h)		
	PVDF	PVDF/SDS–GO	PVDF/SDS–GO/TiO$_2$
1	1.598	3.379	5.845
2	2.237	5.708	9.269
3	3.196	8.037	10.731
4	3.196	9.863	14.064
5	4.566	11.233	16.804
Permeability (L/m^2 h bar)	1.099	2.961	4.187

same final treatment water concentration after the filtration process (0.719–0.724 ppm). The dye rejection efficiency (R) also showed the similar value in the range of 92.76–92.81%. The main difference among the three membranes was the dye flux during filtration. According to Table 4, the highest dye flux was shown by PVDF/SDS–GO/TiO$_2$ (7.770 L/m^2 h) which was caused by high porosity and highest hydrophilicity as proven by contact angle analysis. This

Fig. 6 Measurement of the fabricated NF membrane dye rejection

Table 4 Performance of the fabricated NF membrane measured at the pressure of 2 bar

Membrane	Water flux (L/m^2 h)	Dye flux (L/m^2 h)	Final concentration (ppm)	Rejection rate (%)
PVDF	2.237	1.146	0.721	92.79
PVDF/SDS–GO	5.708	4.476	0.719	92.81
PVDF/SDS–GO/TiO$_2$	9.269	7.770	0.724	92.76

value was approximately fourfold and sevenfold higher than those of PVDF/SDS-GO (4.476 L/ m^2 h) and PVDF samples (1.146 L/m^2 h), respectively. This finding confirmed that the addition of SDS–GO and TiO$_2$ significantly affected the filtration process. The details of the membrane performance for dye rejection are listed in Table 4.

4 Conclusions

Three types of PVDF-based NF membrane were successfully fabricated through phase inversion method. The utilisation of the direct DMAc-based GO synthesised from electrochemical exfoliation assisted by SDS surfactant and TiO$_2$ was proven alter the pore morphology of the fabricated hybrid membrane. Overall, all fabricated membranes presented high MB dye rejection of ~92–93%. However, PVDF/SDS–GO/TiO$_2$ presents the highest hydrophilicity (marked by the lowest contact angle; $64.0 \pm 0.11°$), water permeability (4.187 L/ m^2 h bar) and dye flux (7.770 L/m^2 h; which was sevenfold higher than the pure PVDF membrane). The improvement of membrane morphology and performance was due to the utilisation of both hydrophilic materials in the phase inversion method. This study presents a simpler, less complicated and less time-consuming method to fabricate GO-based PVDF membrane than the presently available methods (the common Hummers' method).

References

Al-gharabli, S., Mavukkandy, M. O., Kujawa, J., Nunes, S. P., & Arafat, H. A. (2017). Activation of PVDF membranes through facile hydroxylation of the polymeric dope. *Journal of Materials Research, 32*(22), 4219–4231.

Balachandran, U., & Eror, N. G. (1982). Raman spectra of titanium dioxide. *Journal of Solid State Chemistry, 42*, 276–282.

Bohara, B. B., Batra, A. K., Arun, K. J., Aggarwal, M. D., & III, C. F. (2017). Fabrication and characterization of polyvinylidene fluoride trifluoroethylene/samarium oxide (Sm$_2$O$_3$) nanocomposite film. *Advanced Science, Engineering and Medicine, 9*, 1–6.

Buonomenna, M. G., Macchi, P., Davoli, M., & Drioli, E. (2007). Poly(vinylidene fluoride) membranes by phase inversion : the role the casting and coagulation conditions play in their morphology, crystalline structure and properties. *European Polymer Journal, 43*, 1557–1572.

Buonomenna, M. G., Choi, S.-H., Galiano, F., & Drioli, E. (2011). Membranes prepared via phase inversion.

Cao, X., Ma, J., Shi, X., & Ren, Z. (2006). Effect of TiO$_2$ nanoparticle size on the performance of PVDF membrane. *Applied Surface Science, 253*, 2003–2010.

Darwish, A. A. A., Rashad, M., & Al-aoh, H. A. (2019). Methyl orange adsorption comparison on nanoparticles: isotherm, kinetics, and thermodynamics studies. *Dyes and Pigments, 160*, 563–571.

Elashmawi, I. S., & Gaabour, L. H. (2015). Raman, morphology and electrical behavior of nanocomposites based on PEO/ PVDF with multi-walled carbon nanotubes. *Results in Physics, 5*, 105–110.

Ghaffar, A., Zhang, L., Zhu, X., & Chen, B. (2018). Porous PVdF/ GO nanofibrous membranes for selective separation and recycling of charged organic dyes from water. *Environmental Science & Technology, 52*(7), 4265–4274.

Hilal, N., Ismail, A. F., Matsuura, T., & Oatley-Radcliffe, D. (2017). Membrane characterization.

Hu, M., & Mi, B. (2013). Enabling graphene oxide nanosheets as water separation membranes. *Environmental Science & Technology, 47*(8), 3715–3723.

Kang, J. H., Kim, T., Choi, J., Park, J., Kim, Y. S., Chang, M. S., et al. (2016). The hidden second oxidation step of Hummers method. *Chemistry of Materials, 28*(3), 756–764.

Kim, J. F., Jung, J. T., Wang, H., Drioli, E., & Lee, Y. (2017). 1.15 Effect of solvents on membrane fabrication via thermally induced phase separation (TIPS): thermodynamic and kinetic perspectives. In *Comprehensive membrane science and engineering II* (Vol. 1, pp. 386–417). Elsevier Ltd.

Kumaran, R., Alagar, M., Kumar, S. D., Subramanian, V., & Dinakaran, K. (2015). Ag induced electromagnetic

interference shielding of Ag-graphite/PVDF flexible nano-composites thinfilms. *Applied Physics Letter, 107*, 113107-1-5.

Liu, J., Fu, X., Cao, D.-P., Mao, L., Wang, J., Mu, D., et al. (2015). Stacked graphene–TiO2 photoanode via electrospray deposition for highly efficient dye-sensitized solar cells. *Organic Electronics, 23*, 158–163.

Madaeni, S. S., & Taheri, A. H. (2011). Effect of casting solution on morphology and performance of PVDF microfiltration membranes. *Chemical Engineering Technology, 34*(8), 1328–1334.

Makertihartha, I. G. B. N., Rizki, Z., Zunita, M., & Dharmawijaya, P. T. (2017). Dyes removal from textile based nanofiltration. *International Seminar on Fundamental and Application of Chemical Engineering, 110006*, 1–8.

Méricq, J.-P., Mendret, J., Brosillon, S., & Faur, C. (2015). High performance PVDF-TiO2 membranes for water treatment. *Chemical Engineering Science, 123*, 283–291.

Mokhtar, N. M., Lau, W. J., Ng, B. C., Ismail, A. F., & Veerasamy, D. (2015). Preparation and characterization of PVDF membranes incorporated with different additives for dyeing solution treatment using membrane distillation. *Desalination and Water Treatment, 56*(8), 1999–2012.

Nasib, A. M., Hatim, I., Jullok, N., & Alamery, H. R. (2017). Morphological properties of poly(vinylidene fluoride-co-tetrafluoroethylene membrane): effect of solvents and polymer concentrations. *Malaysian Journal of Analytical Sciences, 21*(2), 356–364.

Nawi, N. I. M., Bilad, M. R., & Nordin, N. A. H. M. (2018). Effect of dope solution temperature on the membrane structure and membrane distillation performance. IOP Conf. Series: Earth and Environmental Science, 140, 0–7.

Ngang, H. P., Ooi, B. S., Ahmad, A. L., & Lai, S. O. (2012). Preparation of PVDF–TiO2 mixed-matrix membrane and its evaluation on dye adsorption and UV-cleaning properties. *Chemical Engineering Journal, 197*, 359–367.

Nikooe, N., & Saljoughi, E. (2017). Preparation and characterization of novel PVDF nanofiltration membranes with hydrophilic property for filtration of dye aqueous solution. *Applied Surface Science, 413*, 41–49.

Parvez, K., Li, R., Puniredd, S. R., Hernandez, Y., Hinkel, F., Wang, S., et al. (2013). Electrochemically exfoliated graphene as solution-processable, highly conductive electrodes for organic electronics. *ACS Nano, 7*(4), 3598–3606.

Rashad, M., Shaalan, N. M., & Abd-elnaiem, A. M. (2016). Degradation enhancement of methylene blue on ZnO nanocombs synthesized by thermal evaporation technique. *Desalination and Water Treatment, 75*, 26267–26273.

Safarpour, M., Vatanpour, V., Khataee, A., & Esmaeili, M. (2015). Development of a novel high flux and fouling-resistant thin film composite nanofiltration membrane by embedding reduced graphene oxide/TiO2. *Separation and Purification Technology, 154*, 96–107.

Shon, H. K., Phuntsho, S., Chaudhary, D. S., Vigneswaran, S., & Cho, J. (2013). Nanofiltration for water and wastewater treatment–a mini review. *Drinking Water; Engineering and Science, 6*, 47–53.

Suriani, A. B., Nurhafizah, M. D., Mohamed, A., Zainol, I., & Masrom, A. K. (2015). A facile one-step method for graphene oxide/natural rubber latex nanocomposite

production for supercapacitor applications. *Materials Letters, 161*, 665–668.

Suriani, A. B., Nurhafizah, M. D., Mohamed, A., Masrom, A. K., Sahajwalla, V., & Joshi, R. K. (2016). Highly conductive electrodes of graphene oxide/natural rubber latex-based electrodes by using a hyper-branched surfactant. *Materials & Design, 99*, 174–181.

Suriani, A. B., Fatiatun, Mohamed, A., Muqoyyanah, Hashim, N., Rosmi, M. S., et al. (2018a). Reduced graphene oxide/platinum hybrid counter electrode assisted by custom-made triple-tail surfactant and zinc oxide/titanium dioxide bilayer nanocomposite photoanode for enhancement of DSSCs photovoltaic performance. *Optik-International Journal for Light and Electron Optics, 161*, 70–83.

Suriani, A. B., Muqoyyanah, Mohamed, A., Mamat, M. H., Hashim, N., Isa, I. M., et al. (2018b). Improving the photovoltaic performance of DSSCs using a combination of mixed-phase TiO2 nanostructure photoanode and agglomerated free reduced graphene oxide counter electrode assisted with hyperbranched surfactant. *Optik - International Journal for Light and Electron Optics, 158*(2010), 522–534.

Suriani, A. B., Muqoyyanah, Mohamed, A., Othman, M. H. D., Mamat, M. H., Hashim, N., et al. (2018c). Reduced graphene oxide-multiwalled carbon nanotubes hybrid film with low Pt loading as counter electrode for improved photovoltaic performance of dye-sensitised solar cells. *Journal of Materials Science: Materials in Electronics, 29*(13), 10723–10743.

Thürmer, M. B., Poletto, P., Marcolin, M., Duarte, J., & Zeni, M. (2012). Effect of non-solvents used in the coagulation bath on morphology of PVDF membranes. *Materials Research, 15*(6), 884–890.

Thuyavan, Y. L., Anantharaman, N., Arthanareeswaran, G., & Ismail, A. F. (2016). Impact of solvents and process conditions on the formation of polyethersulfone membranes and its fouling behavior in lake water filtration. *Journal of Chemical Technology & Biotechnology, 91*(10), 2568–2581.

Wang, X., Zhang, L., Sun, D., An, Q., & Chen, H. (2008). Effect of coagulation bath temperature on formation mechanism of poly (vinylidene fluoride) membrane. *Journal of Applied Polymer Science, 110*, 1656–1663.

Wang, Z., Yu, H., Xia, J., Zhang, F., Li, F., Xia, Y., & Li, Y. (2012). Novel GO-blended PVDF ultrafiltration membranes. *Desalination, 299*, 50–54.

Xu, Z., Zhang, J., Shan, M., Li, Y., Li, B., Niu, J., et al. (2014). Organosilane-functionalized graphene oxide for enhanced antifouling and mechanical properties of polyvinylidene fluoride ultrafiltration membranes. *Journal of Membrane Science, 458*, 1–13.

Yu, P., Lowe, S. E., Simon, G. P., & Zhong, Y. L. (2015). Electrochemical exfoliation of graphite and production of functional graphene functional graphene. *Current Opinion in Colloid & Interface Science, 20*(5–6), 329–338.

Yusoff, I. I., Rohani, R., Zaman, N. K., Junaidi, M. U. M., Mohammad, A. W., & Zainal, Z. (2018). Durable pressure filtration membranes based on polyaniline–polyimide P84 blends. *Polymer Engineering and Science*, 1–11.

Zhang, P., Gong, J., Zeng, G., Deng, C., Yang, H., Liu, H., & Huan, S. (2017). Cross-linking to prepare composite graphene oxide-framework membranes with high-flux for dyes and heavy metal ions removal. *Chemical Engineering Journal, 322*, 657–666.

Zhao, Y., Xu, Z., Shan, M., Min, C., Zhou, B., Li, Y., et al. (2013). Effect of graphite oxide and multi-walled carbon nanotubes on the microstructure and performance of PVDF membranes. *Separation and Purification Technology, 103*, 78–83.

Zhou, M., Tang, J., Cheng, Q., Xu, G., Cui, P., & Qin, L. C. (2013). Few-layer graphene obtained by electrochemical exfoliation of graphite cathode. *Chemical Physics Letters, 572*, 61–65.

Zhu, Z., Wang, L., Xu, Y., Li, Q., Jiang, J., & Wang, X. (2017). Preparation and characteristics of graphene oxide-blending PVDF nanohybrid membranes and their applications for hazardous dye adsorption and rejection. *Journal of Colloid and Interface Science, 504*, 429–439.

Zinadini, S., Zinatizadeh, A. A., Rahimi, M., Vatanpour, V., & Zangeneh, H. (2014). Preparation of a novel antifouling mixed matrix PES membrane by embedding graphene oxide nanoplates. *Journal of Membrane Science, 453*, 292–301.